CFD Validation for Hypersonic Flight: Real Gas Flows

Graham V. Candler*
Ioannis Nompelis**

Aerospace Engineering and Mechanics & Army HPC Research Center
University of Minnesota, Minneapolis MN 55455

Abstract

The aerodynamics of future hypersonic air-breathing vehicles will be greatly affected by high-enthalpy or "real gas" effects. It is the purpose of a recent NATO Research and Technology Organization study to assess the readiness of computational fluid dynamics to simulate high-enthalpy flows. This paper summarizes the results of this effort through the discussion of four test cases: a transverse cylinder, shock-shock interactions, blunt double-cones, and a large blunt cone-flare. The contributed CFD results are capable of capturing the main features of these flows, but quantitative comparisons are probably not sufficiently accurate for vehicle design. The study also shows that there are too few reliable high-enthalpy datasets to validate CFD codes.

Introduction

The NATO countries have formed a group called the Research and Technology Organization (RTO) that replaces AGARD. Within RTO, there is Working Group 10: Technologies for Propelled Hypersonic Vehicles. One of the activities of this working group is the validation of CFD codes and flow models for hypersonic flows. Prof. Doyle Knight of Rutgers University heads this activity. A component of the code validation activity involves the simulation of high-enthalpy flows, or real gas flows. These flows have substantial levels of chemical reactions and internal energy excitation. It is the intention of this part of the code validation activity to determine whether current CFD models and methods can accurately predict high-enthalpy flows for hypersonic vehicle simulations.

This paper discusses the results of this code validation study by making comparisons between experiments and CFD simulations of several high-enthalpy flows. As such, only well characterized experiments are used for the test cases, which include a finite-length cylinder transverse to the flow, shock-shock interactions on a cylindrical leading edge, blunt double-cones, and a large blunt cone-flare. Computations were submitted for all but the last of these cases. However, only two groups submitted results.

The remainder of this paper summarizes each test case, briefly discusses the numerical methods used to simulate the flow, and then evaluates the accuracy of the computed results. Based on the results, an assessment of the readiness of CFD for the simulation of hypersonic reacting flows is given. A related issue is whether the free-stream conditions in the present high-enthalpy facilities are sufficiently well characterized for code validation.

Dataset No. 1:
Circular Cylinder

This test case consists of a 90 mm diameter, 380 mm long cylinder placed transverse to a high-enthalpy flow of air in the HEG facility. The nozzle exit conditions are supplied by separate computations discussed in Ref. 1. A circular cylinder flow has several advantages over other test geometries: line-of-sight symmetry, no complicated flow interactions, and a large standoff distance to diameter ratio. This simplifies the use of optical measurement techniques, and provided that the flow field is truly two-dimensional, CFD simulations are straight-forward. The final experimental results are not yet available, so we are only able to use CFD results to study the possible three-dimensionality of the flow fields.

Contributed Calculations

Our research group made the only contribution for this test case. The higher enthalpy (21.7 MJ/kg) condition was used for our calculations; these conditions are:

Condition I: Air at $p_\infty = 660\,\mathrm{Pa}$, $T_\infty = 1140\,\mathrm{K}$, $u_\infty = 5940\,\mathrm{m/s}$, with mass fractions of $c_{\mathrm{N_2}} = 0.745$, $c_{\mathrm{O_2}} = 0.047$, $c_{\mathrm{NO}} = 0.0293$, $c_{\mathrm{N}} = 4.6 \times 10^{-9}$, $c_{\mathrm{N}} = 0.178$.

The CFD calculations used a three-dimensional parallel implicit code[2] to model the finite-length grid using a grid of size $60 \times 60 \times 90$ in the spanwise, cir-

* Professor, AIAA Associate Fellow (candler@aem.umn.edu)
** Graduate Research Assistant, AIAA Student Member

Report Documentation Page

Form Approved
OMB No. 0704-0188

1. REPORT DATE	2. REPORT TYPE	3. DATES COVERED
01 JAN 2006	**N/A**	**-**

4. TITLE AND SUBTITLE
CFD Validation for Hypersonic Flight: Real Gas Flows

5a. CONTRACT NUMBER
5b. GRANT NUMBER
5c. PROGRAM ELEMENT NUMBER

6. AUTHOR(S)

5d. PROJECT NUMBER
5e. TASK NUMBER
5f. WORK UNIT NUMBER

7. PERFORMING ORGANIZATION NAME(S) AND ADDRESS(ES)
Aerospace Engineering and Mechanics & Army HPC Research Center University of Minnesota, Minneapolis MN 55455

8. PERFORMING ORGANIZATION REPORT NUMBER

9. SPONSORING/MONITORING AGENCY NAME(S) AND ADDRESS(ES)

10. SPONSOR/MONITOR'S ACRONYM(S)

11. SPONSOR/MONITOR'S REPORT NUMBER(S)

12. DISTRIBUTION/AVAILABILITY STATEMENT
Approved for public release, distribution unlimited

13. SUPPLEMENTARY NOTES
See also ADM001860, Technologies for Propelled Hypersonic Flight (Technologies des vols hypersoniques propulses). , The original document contains color images.

14. ABSTRACT

15. SUBJECT TERMS

16. SECURITY CLASSIFICATION OF:			17. LIMITATION OF ABSTRACT	18. NUMBER OF PAGES	19a. NAME OF RESPONSIBLE PERSON
a. REPORT	b. ABSTRACT	c. THIS PAGE			
unclassified	**unclassified**	**unclassified**	**UU**	**10**	

Standard Form 298 (Rev. 8-98)
Prescribed by ANSI Std Z39-18

cumferential, and normal directions. In addition, two-dimensional calculations were performed on a much finer grid to assess the effects of three-dimensionality on the measured results. The thermo-chemical model used was a five-species, five-reaction air kinetics model with vibrational nonequilibrium and the Park $\sqrt{TT_v}$ vibration-dissociation coupling model.[3] Millikan and White vibrational relaxation rates and the Park 1988 reaction rates were used.[4]

Figure 1 plots a schematic of the grid used in the calculation, showing the two planes of symmetry and the outflow plane. Note the large length to diameter ratio. Figure 2 plots the computed density contours in the plane of symmetry located at the cylinder centerline. These contour shapes are consistent with those reported by Hornung for nitrogen flows over finite-length cylinders.[5] There are notable differences between the computed contours, even at this plane far from the cylinder end. Figure 3 plots the computed density along the stagnation streamline, along with two-dimensional results. The density profiles agree with each other fairly well, with the three-dimensionality causing a more gradual rise in the density at the shock wave.

The experiments use a line-of-sight integration along the cylinder axis to determine the density profile on the stagnation streamline. Therefore, any curvature in the bow shock wave due to the shock wrapping around the ends of the cylinder will change the measured density profile. The magnitude of this effect may be assessed with Fig. 4, which plots the contours of density in the plane that passes through the leading edge of the cylinder. The shock standoff distance decreases within about one cylinder radius of the cylinder end. This is reflected in Fig. 5, which are synthetic interferograms constructed from the 2D and 3D CFD flow fields. The interferograms are similar, but note that in the 3D case the shock standoff distance appears to be larger. This is likely a result of insufficient grid resolution in the vicinity of the bow shock; future grid resolution studies will verify this conjecture. There are noticeable differences in the fringe shapes in the two calculations; the 3D results tend to have a more curved shape at the downstream end of each fringe. Thus to validate a CFD code, a 3D calculation is required.

An additional possible source of error in the measurements for this test case involves the uniformity of the free-stream flow conditions. The large size of the model will reduce random non-uniformities in the test conditions, but the scale would tend to increase the importance of systematic variations in the test-section flow.

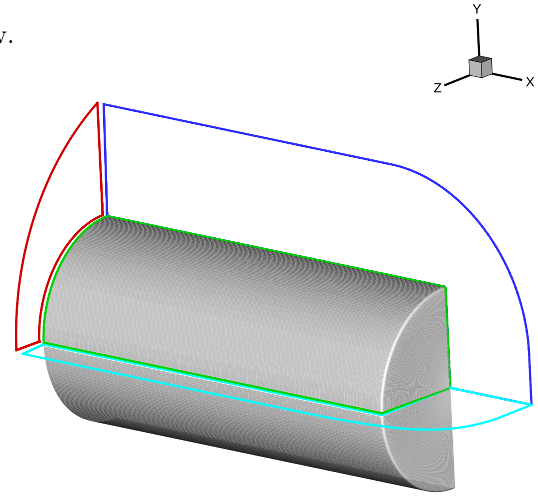

FIGURE 1. Schematic of 3D finite-length cylinder grid.

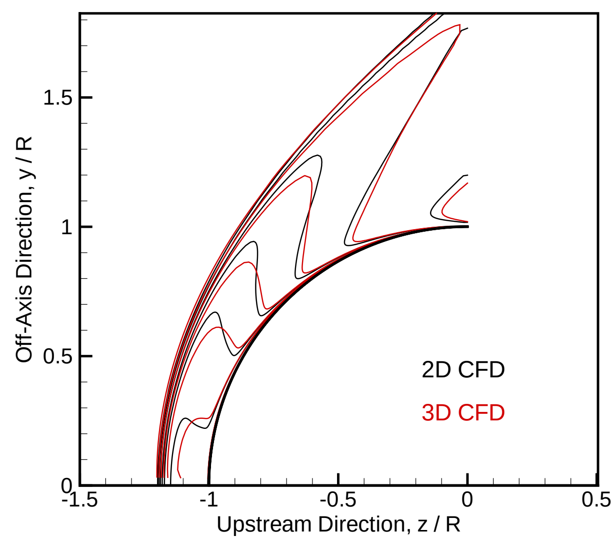

FIGURE 2. Computed density contours in the cylinder mid-plane at HEG condition 1.

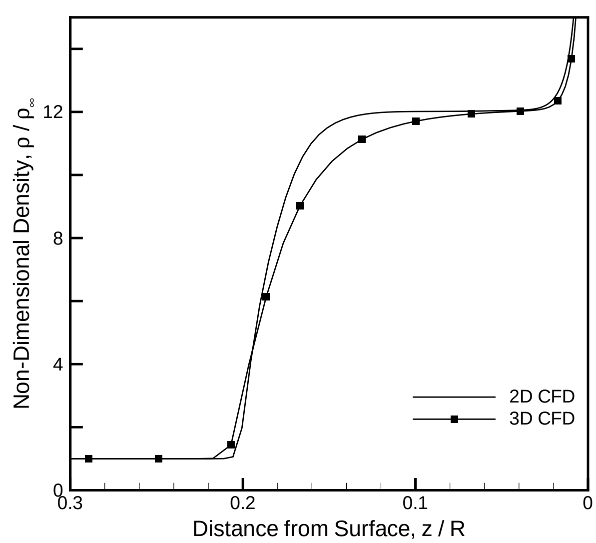

FIGURE 3. Computed density variation along the stagnation streamline located at the cylinder midpoint.

Also plotted is the density computed assuming a two-dimensional flow.

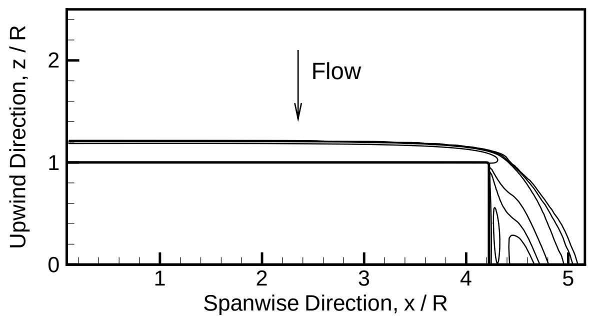

FIGURE 4. Computed density contours in the plane through the cylinder leading edge; note curvature of bow shock near cylinder end.

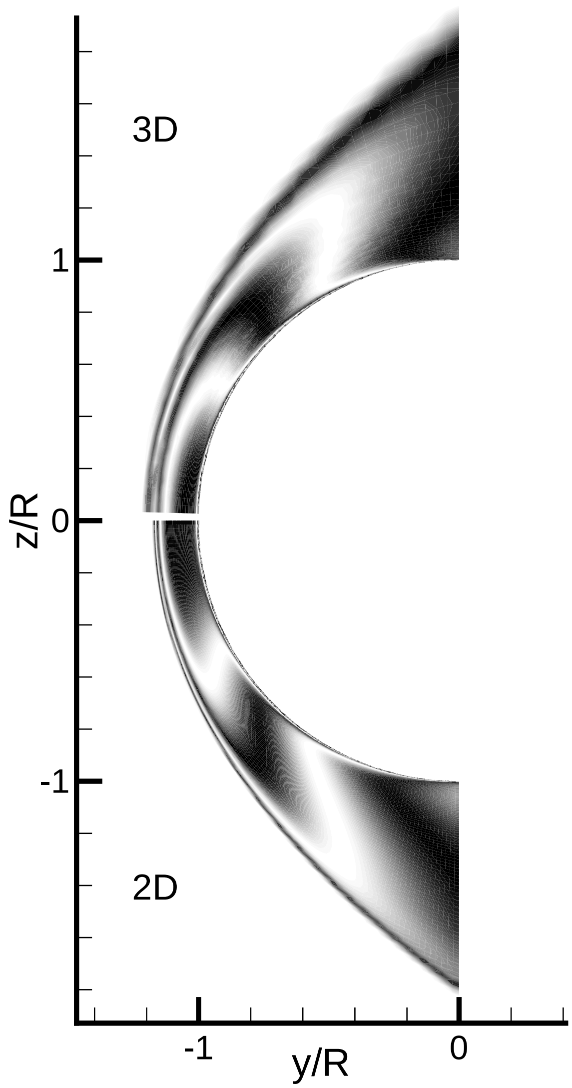

FIGURE 5. Synthetic interferograms constructed using a line-of-sight integration through the flow field from two- and three-dimensional CFD computations.[6]

Dataset No. 2:

Shock-Shock Interaction on a Cylindrical Leading Edge

This test case consists of a 3 inch diameter cylinder placed transverse to a high-enthalpy flow in the LENS facility.[7] A planar shock is generated upstream of the cylinder, and this shock interacts with the bow shock on the cylinder. The position of the cylinder is adjusted until a strong Edney Type IV interaction is obtained.

This flow is motivated by the question as to whether chemical reaction effects enhance the heat transfer and pressure levels in shock interactions. In these experiments, models with a high spatial resolution of heat transfer and pressure gages were used. Measurements were made in both air and nitrogen flows and the experiments indicate a significant enhancement of the amplification factors in the interaction regions.[7]

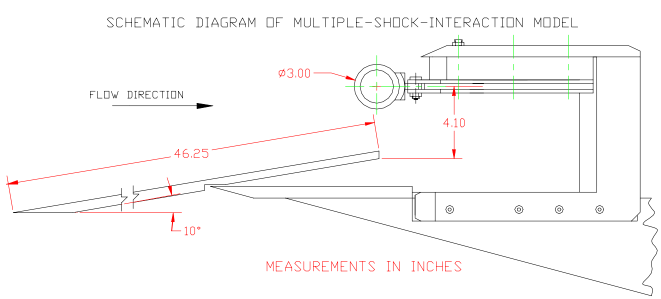

FIGURE 6. Schematic of real gas shock-shock interaction model. From Refs. 7 and 8.

Contributed Calculations

Our research group made the only contribution for this test case. There are two available runs in the LENS facility: Run 48 which is nitrogen at 10.5 MJ/kg, and Run 50 which is air at 11.3 MJ/kg. The test section conditions were supplied by Holden as:

Run 48: Nitrogen at $\rho_\infty = 3.42\,\mathrm{g/cm^3}$, $T_\infty = 556\,\mathrm{K}$, $u_\infty = 4450\,\mathrm{m/s}$.

Run 50: Air at $\rho_\infty = 3.30\,\mathrm{g/cm^3}$, $T_\infty = 672\,\mathrm{K}$, $u_\infty = 4480\,\mathrm{m/s}$.

No information was given about the computed level of reaction in the test section; therefore, we assumed that the flow was in equilibrium.

The computations used a 382×256 grid on $180°$ of the cylinder. The same parallel implicit CFD code listed above was used with a 5-species model for air and a 2-species model for nitrogen. We used oblique shock relations with a frozen flow assumption to obtain the conditions downstream of the shock generator. The geometry shown in Fig. 5 was used to estimate the location of the shock impingement on the cylinder bow shock. However, we found that the resulting interaction did not occur at the same location as predicted by the data. We therefore adjusted the location of the impingement location to better match the peak heat transfer rate in the experiments. This approach was suggested by Holden and only resulted in a small adjustment of the impingement location. It should be noted that the shock generator is very large, and even a small change in its location results in a significant change in the shock impingement point. This then results in a large change in the pressure and heat transfer distributions.

The comparisons between the CFD and experimental data are somewhat encouraging, and are consistent between the two runs. For the N_2 run, the heat transfer rate prediction is fairly reasonable, except that the CFD predicts a 40% higher peak than the experiments. Also, the heat transfer near the cylinder leading edge is generally under-predicted. On the other hand, the pressure distribution is very poorly predicted, with the computed peak over 3 times higher and offset further around the cylinder than measured.

Figure 8 shows that the air run has a similar result, with the predicted pressure about 3 times larger than measured. Again, the pressure peak is broader in the experiments. If we use a non-catalytic surface boundary condition, as in the nitrogen case, the computations under-predict the measured heat transfer rate by about 40%. However, because this is an air flow over a metal model, it is likely that the surface promotes recombination of the oxygen molecules. Therefore, as a bounding calculation to assess the effects of wall catalysis, we used a super-catalytic surface. This means that the gas is assumed to recombine completely at the surface. With this boundary condition, we get remarkably good agreement between the computations and experiments. Again, we obtain poor agreement between the computations and the cluster of heat transfer gages located near the zero angle (leading edge) location.

It should be noted that these experiments are difficult, with the shock interaction point occurring over a very small angular extent. Thus there is inherently smoothing of the data in the regions of high pressure and heat transfer rate gradients. Also, any small variation in the free-stream conditions translates into apreciably movement of the impinging shock relative to the bow shock. In addition, other measurements and computations of Type IV interactions have shown the possible presence of inherent unsteadiness in the interaction. Thus, it is quite likely that the interaction is sweeping over the surface, resulting in a broadening of the peak as seen in Run 48.

Therefore, we conclude from these comparisons that the computations are in reasonable agreement with the experiments. However, the CFD predicts significantly higher pressures and heat transfer rates in the vicinity of the interaction. This is likely due to some level of unsteadiness in the experiments which causes a broadening of the jet impingement. Clearly, the effects of wall catalysis are important and should be further investigated at the test conditions.

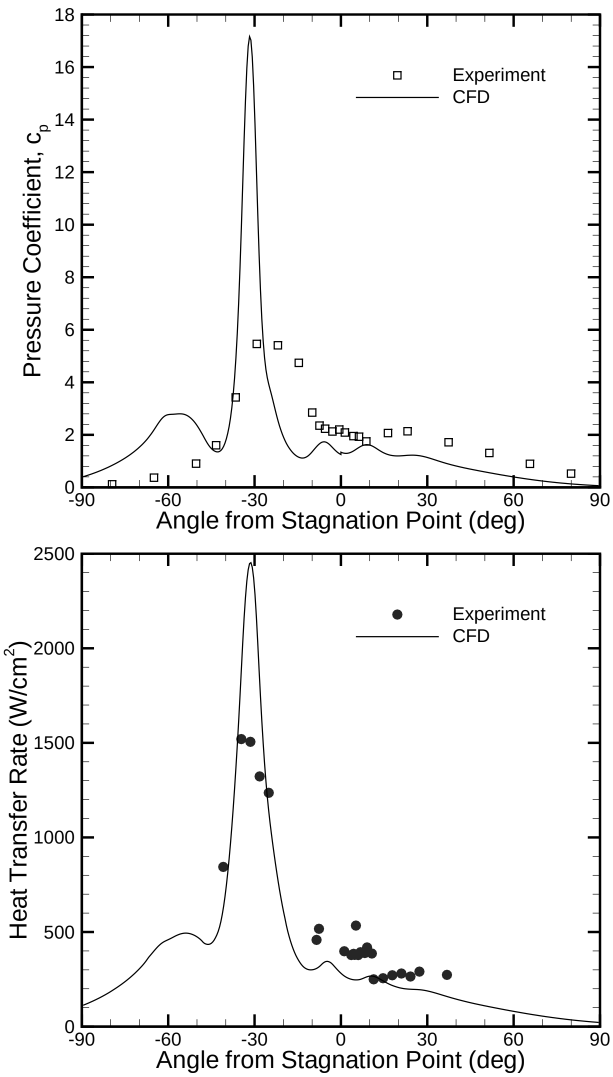

FIGURE 7. Surface pressure coefficient and heat transfer rate on cylinder at Run 48 conditions (10.5 MJ/kg

N_2).

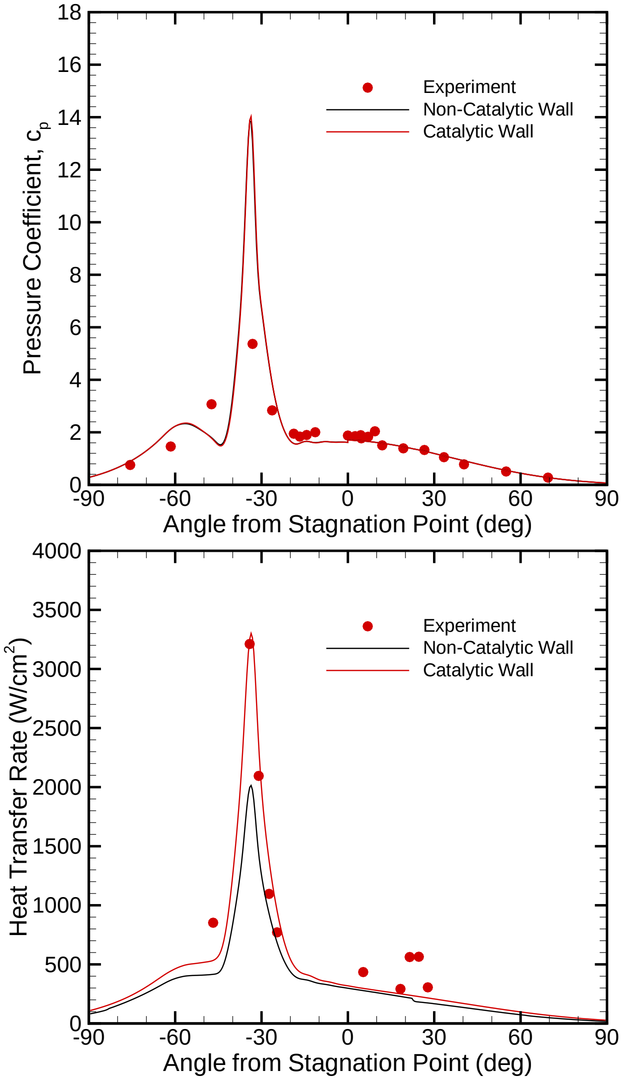

FIGURE 8. Surface pressure coefficient and heat transfer rate on cylinder at Run 50 conditions (11.3 MJ/kg Air).

Dataset No. 3: Blunt Cone-Flare

This test case is similar to several of those that make up the Laminar Viscous-Inviscid Interaction test cases.[9] However for the present runs, the enthalpy was higher so that there would be significant levels of chemical reaction, and the second cone angle was larger (60° instead of 55°). Numerical studies have shown that this configuration is very sensitive to chemical reaction effects. Thus, in principle, this test case should yield important code validation information.

The model is shown in Fig. 9, and was highly instrumented with high-frequency heat transfer and pressure gages. Measurements were made to obtain the distribution of the surface quantities, the separation zone size, and information about any high-frequency oscillations that might occur. Test conditions were in air and nitrogen at nominally 5 and 10 MJ/kg with reservoir pressures of between 270 and 500 bar.

Contributed Calculations

Two research groups contributed results to this test case. The group of Drs. Marco Marini and Salvatore Borelli from the Italian Aerospace Research Center (CIRA) performed a large and careful study of this problem. My research group made a much more limited analysis of one test case.

Marini and Borelli ran calculations at four test conditions, and we simulated Run 46, which is the high-enthalpy air case. The test section conditions were supplied by Holden as:

Run 42: Air at $\rho_\infty = 5.67\,\mathrm{g/cm^3}$, $T_\infty = 224\,\mathrm{K}$, $u_\infty = 3170\,\mathrm{m/s}$.

Run 44: N_2 at $\rho_\infty = 5.82\,\mathrm{g/cm^3}$, $T_\infty = 242\,\mathrm{K}$, $u_\infty = 3320\,\mathrm{m/s}$.

Run 45: N_2 at $\rho_\infty = 3.31\,\mathrm{g/cm^3}$, $T_\infty = 556\,\mathrm{K}$, $u_\infty = 4450\,\mathrm{m/s}$.

Run 46: Air at $\rho_\infty = 3.28\,\mathrm{g/cm^3}$, $T_\infty = 672\,\mathrm{K}$, $u_\infty = 4480\,\mathrm{m/s}$.

Marini and Borelli used grids of 144×40, 216×60 and 288×80; we used a grid of 512×256 points. The CIRA researchers used a flux difference splitting Riemann solver with second-order reconstruction of the fluxes at the finite volume faces. Their time integration used an explicit multistage Runge-Kutta method with global or local time stepping. Our calculations used the same parallel implicit finite-volume method discussed above. Very similar thermo-chemical models were used by both groups; these have also been discussed above.

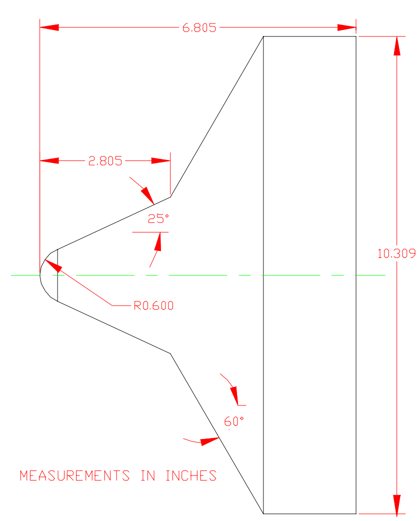

FIGURE 9. Schematic of blunt cone-flare model. From Refs. 7 and 8.

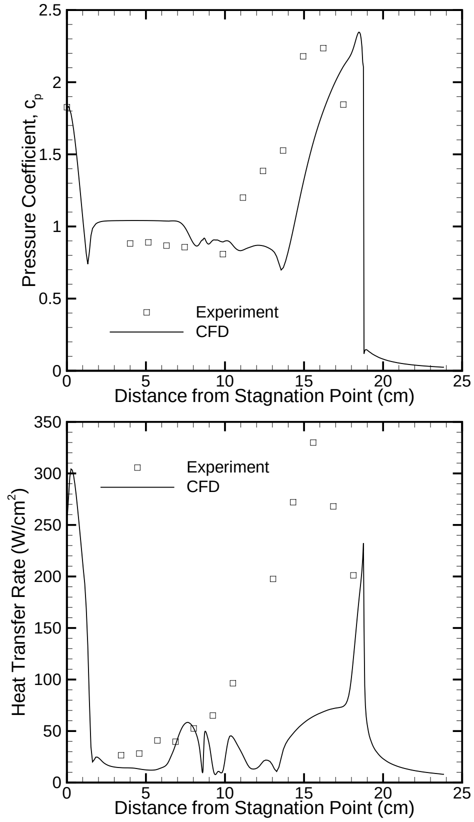

FIGURE 10. Marini and Borelli surface pressure and heat transfer rate results for Run 42.

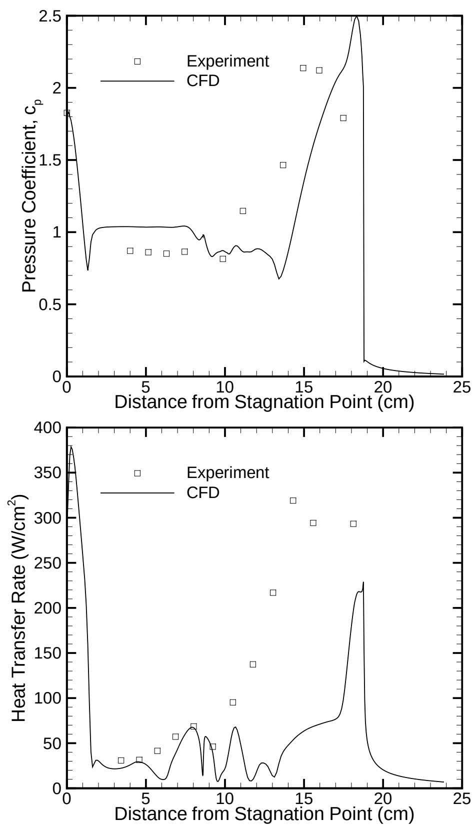

FIGURE 11. Marini and Borelli surface pressure and heat transfer rate results for Run 44.

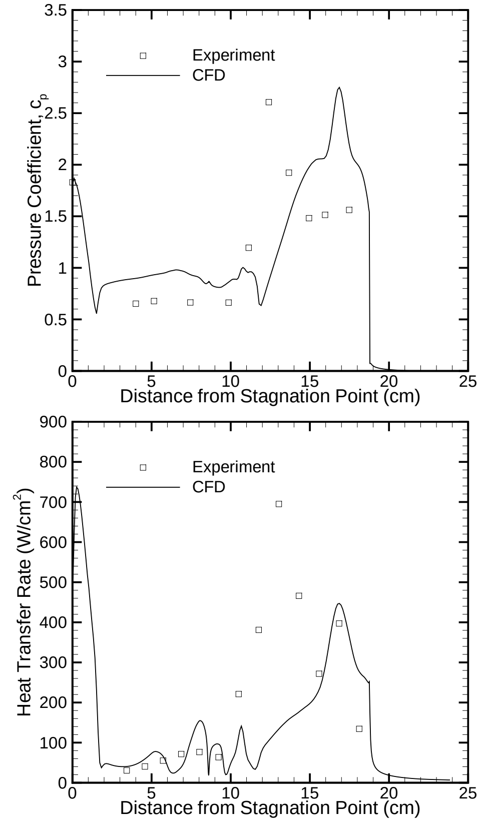

FIGURE 12. Marini and Borelli surface pressure and heat transfer rate results for Run 45.

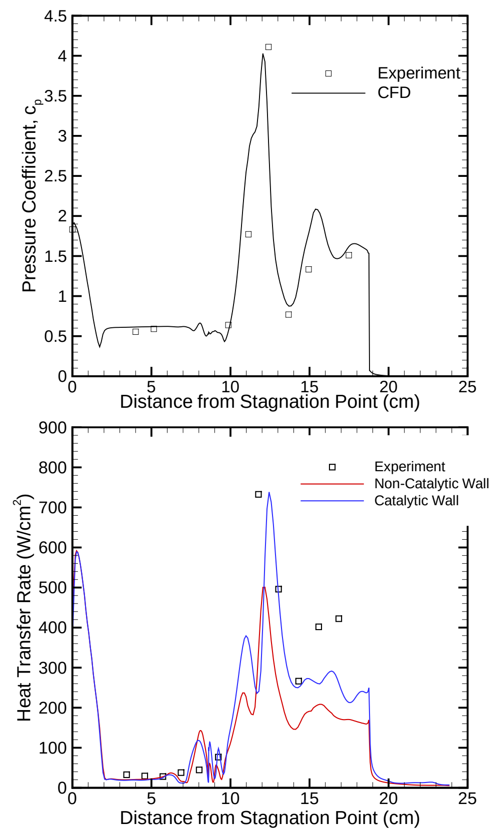

FIGURE 13. Marini and Borelli surface pressure and heat transfer rate results for Run 46.

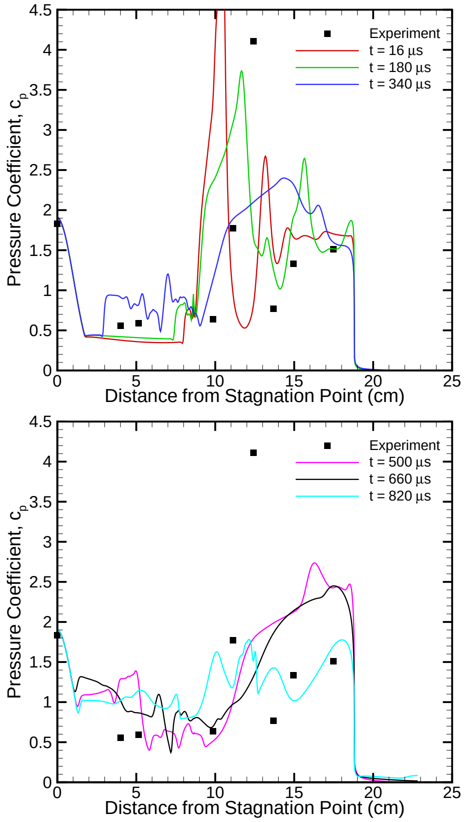

FIGURE 14. Candler group surface pressure as a function of the elapsed flow time for Run 46.

Figures 10-13 summarize the results of the Marini and Borelli analysis of this dataset. Generally, the agreement between the computations and experiments is reasonable for the surface pressure, but there is a significant difference in the predicted heat transfer rates for three of the cases. The computations agree best for Run 46, which is the high enthalpy air case. The pressure comparison is remarkably good, with all of the flow features captured. The predicted heat transfer rate is low, but Marini and Borelli recognized that at these conditions the surface may be catalytic. Therefore, they simulated Run 46 with a super-catalytic surface downstream of the cone-cone juncture. These results plotted in Fig. 13 show very good agreement with the experimental heat transfer rate data.

The CIRA computations predict an apparently steady flow, with some unsteadiness in the separation zone for the high Reynolds number, low enthalpy cases. This lack of large-scale unsteadiness is in agreement the experimental observations.

The results of the Candler group calculations are more difficult to present because we were unable to obtain steady-state results. This may be a result of the numerical method, our finer grid, or some other effect. Figure 14 summarizes our results for Run 46; we plot the computed surface pressure as a function of the elapsed flow time in the calculations. At a time of 180 μsec, the agreement between the CFD and experiments is quite reasonable, and is similar to the CIRA results. However, if we continue to run the calculation, we find that the flow breaks down and becomes massively unsteady. This is reflected in the wildly varying pressure variation plotted in Fig. 13. At this point, we do not know why our calculations predict this highly unsteady flow for this case, while the CIRA computations and the experiments are steady.

Dataset No. 4: Large Blunt Cone-Flare

Two sets of studies were conducted with the large blunt cone-flare geometry shown in Fig. 15. The model was highly instrumented with heat transfer and pressure gages to obtain detailed surface distributions for a range of free-stream conditions at velocities between 3 km/sec to 4.5 km/sec at reservoir pressures of 500 MPa, for both nitrogen and air flows. These conditions were selected to explore the effects of the Reynolds number and enthalpy on the flow field. The large scale of the model may have resulted in sufficiently large Reynolds numbers to cause transition in the shear layer of the separation zone.

Four test conditions were run by Holden and the experimental data are available in Refs. 9 and 11. However, to date there have been no submissions for this test case. This is a challenging case to compute because of the high Reynolds numbers and large scale of the model, however it is a useful test case that should be examined.

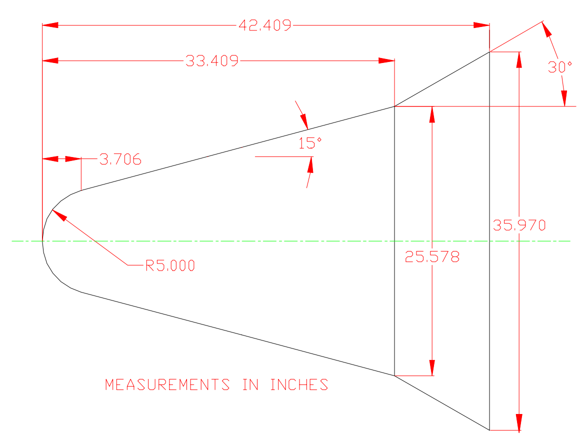

FIGURE 15. Schematic of large blunt cone-flare model. From Refs. 6, 7.

Discussion and Conclusions

The code validation study for high-enthalpy real-gas flows has not been very successful in several ways. Only two research groups participated in the study and as a result, only two test cases were compared with data. These comparisons are at enthalpies of up to 11.3 MJ/kg in air, which corresponds to a flight speed of about 4.7 km/s or a Mach number of about 15 in the atmosphere. Thus, these conditions are consistent with likely air-breathing flight conditions. However, there are limited data available and this makes it difficult to "validate" the existing computational fluid dynamics methods and thermo-chemical models.

The finite-length cylinder test case has the potential to be useful for code validation. It appears that the interferograms are weakly affected by three-dimensionality. But, three-dimensional reacting flow simulations are no longer challenging, and it is easier to account for this effect than for many of the other uncertainties in high-enthalpy flows. Because the cylinder affords more accurate and sensitive measurements of the density field than a sphere for example, it is probably the best geometry for blunt-body test cases.

The shock-shock interaction study shows reasonable agreement with the experiments, given the complexity of this flow. The CFD simulations show a much stronger amplification factor for the pressure than measured in the experiments. But this is consistent with slight unsteadiness in the interaction and the free-stream conditions. The importance of the gas-surface interaction model was clearly illustrated in the air experiment. Wall catalysis plays a significant role at these test conditions.

The blunt double cone flows are puzzling, in that there is good agreement between the calculations of Marini and Borelli for Run 46. But my group's calculation shows a strong unsteadiness in the flow field.

Performing validation quality experiments at these conditions is very difficult. The facilities are impulse facilities and compress the working gas to very high pressures and temperatures before the expansion to the test-section conditions. We have found that at enthalpies of only about 3 MJ/kg in nitrogen, the test-section conditions are significantly affected by vibrational freezing near the throat conditions.[10] This results in test conditions at a lower axial velocity and higher density than expected. Clearly, at these much higher enthalpies there will be vibrational as well as chemical freezing in the nozzle, which will alter the test conditions. This effect is probably not very important for blunt body flows, but will be very important for more complex flows such as those studied in Ref. 10. Unfortunately, the modeling of high-enthalpy expansions of air is very difficult and likely requires additional research.

From this study, it is also clear that we need more contributors to the real gas test cases. Additional test cases are needed, either from the existing literature or some new experiments need to be performed. Careful thought must be given to the design of new experiments, which should be coupled with a complete analysis of the experimental facilities, including a CFD study of the nozzle flow and advanced diagnostics to characterize the free-stream.

Based on these comments, it is not really possible to say that CFD codes are validated for real-gas flows. These flows are so complicated, that the notion that we can "validate" a code for high-enthalpy flows is over-simplified. Each experiment has its own idiosyncracies, and it is very difficult to separate them from the data. Clearly, CFD can simulate many flows with a reasonable degree of confidence, but we don't have a good understanding of where the models break down.

Acknowledgments

We would like to thank Dr. Joseph Olejniczak for constructing the interferograms presented in this work. This work was sponsored by the Air Force Office of Scientific Research under grant AF F49620-01-1-0088. The views and conclusions contained herein are those of the authors and should not be interpreted as necessarily representing the official policies or endorsements, either expressed or implied, of the AFOSR or the U.S. Government. This work is also sponsored in part by the Army High Performance Computing Research Center under the auspices of the Department of the Army, Army Research Laboratory cooperative agreement number DAAD191-01-2-0014, the content of which does not necessarily reflect the position or the policy of the government, and no official endorsement should be inferred. A portion of the computer time was provided by the University of Minnesota Supercomputing Institute.

References

[1] Hannemann, K., B. Reimann, J. Martinez Schramm and M. Schnieder, "The Influence and the Delay of Driver Gas Contamination in HEG," *AIAA Paper 2000-2593,* June 2000.

[2] Wright, M.J., D. Bose, and G.V. Candler, "A Data-Parallel Line Relaxation Method for the Navier-Stokes Equations," *AIAA Journal,* Vol. 36, No. 9, pp. 1603-1609, Sept. 1998.

[3] Park, C., "Assessment of Two-Temperature Kinetic Model for Ionizing Air," *AIAA Paper No. 87-1574,*

June 1987.

4 Park, C., "Two-Temperature Interpretation of Dissociation Rate Data for N_2 and O_2," *AIAA Paper No. 88-0548,* Jan. 1988.

5 Hornung, H.G., "Non-equilibrium Dissociating Nitrogen Flow Over Spheres and Circular Cylinders," *J. Fluid Mechanics,* Vol. 53, pp. 149-176, 1972.

6 Olejniczak, J., "Computational and Experimental Study of Nonequilibrium Chemistry in Hypersonic Flows," University of Minnesota Ph.D. Thesis, Apr. 1997.

7 Holden, M.S., "Shock Interaction Phenomena in Hypersonic Flows," *AIAA Paper No. 98-2751*, June 1998.

8 Holden, M.S., "Experimental Database from CUBRC Studies in Hypersonic Laminar and Turbulent Interacting Flows Including Flowfield Chemistry," Calspan-University at Buffalo Research Center, Dec. 2000.

9 Holden, M.S., and J.K. Harvey, "Comparisons Between DSMC and Navier-Stokes Solutions on Measurements in Regions of Laminar Shock Wave Boundary Layer Interaction in Hypersonic Flows," *AIAA Paper No. 2002-0435*, Jan. 2002.

10 Candler, G., I. Nompelis, M.-C. Druguet, M.S. Holden, T.P. Wadhams, I. Boyd and W.-L. Wang, "CFD Validation for Hypersonic Flight: Hypersonic Double-Cone Flow Simulations," *AIAA Paper No. 2002-0581,* Jan. 2002.

11 Holden, M.S., R. Bergman, J. Harvey, I. Boyd, J. George, "Experimental Studies of Real Gas Effects Over a Blunted Cone/Flare Configuration in Hypervelocity Flows," *AIAA Paper No. 97-0855,* Jan. 1997.